

Stabilizing Single Ni Adatoms on a Two-Dimensional Porous Titania Overlayer at the SrTiO₃(110) Surface

Zhiming Wang*,† Xianfeng Hao,† Stefan Gerhold,† Petr Mares,†,|| Margareta Wagner,† Roland Bliem,† Karina Schulte,‡ Michael Schmid,† Cesare Franchini,§ and Ulrike Diebold*,†

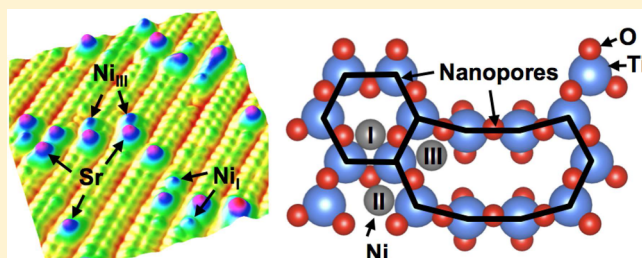
[†]Institute of Applied Physics, Vienna University of Technology, Wiedner Hauptstraße 8-10, 1040 Vienna, Austria

[‡]MAX IV Laboratory, Lund University, Ole Römers väg 1, 223 63 Lund, Sweden

[§]Faculty of Physics and Center for Computational Materials Science, University of Vienna, Sensengasse 8/12, 1090 Vienna, Austria

^{||}CEITEC BUT, Technicka 10, 61669 Brno, Czech Republic

ABSTRACT: Nickel vapor-deposited on the SrTiO₃(110) surface was studied using scanning tunneling microscopy, photoemission spectroscopy (PES), and density functional theory calculations. This surface forms a (4 × 1) reconstruction, composed of a 2-D titania structure with periodic six- and ten-membered nanopores. Anchored at these nanopores, Ni single adatoms are stabilized at room temperature. PES measurements show that the Ni adatoms create an in-gap state located at 1.9 eV below the conduction band minimum and induce an upward band bending. Both experimental and theoretical results suggest that Ni adatoms are positively charged. Our study produces well-dispersed single-adatom arrays on a well-characterized oxide support, providing a model system to investigate single-adatom catalytic and magnetic properties.



INTRODUCTION

Scanning probe microscopy studies of single adatoms on surfaces have revealed novel physical phenomena.^{1,2} In addition, single-metal adatoms on oxide supports have shown remarkable performance in catalytic reactions.^{3–6} Approaches to produce single-metal adatom arrays include mass-selected soft-landing, wet-chemistry approaches, as well as vapor deposition in ultrahigh vacuum (UHV) conditions.^{3,7,8} However, stabilizing single atoms on oxide supports has remained a significant challenge because sintering occurs under realistic reaction conditions.^{9–11} Special sites such as defects, moiré patterns, and reconstructions with strong modulation of surface potential⁸ make it possible to anchor and stabilize single-metal adatoms. Recently, Freund and coworkers have demonstrated that a 2D porous silica structure grown on metal substrates is a suitable candidate for stabilizing single adatoms such as Li, Fe, Ag, and Pd.^{12–14} This silica structure is composed of a single layer of corner-sharing SiO₄ tetrahedra that form six-membered rings of 5 Å diameter.¹⁵ Here we introduce a 2D porous titania structure on SrTiO₃ that can serve as a template for single-metal adatoms.

Strontium titanate (SrTiO₃), the prototypical perovskite oxide, has attracted extensive interest.^{16–21} Surface reconstructions on various SrTiO₃ faces often consist of porous 2D titania structures.^{22–25} For the (110) orientation, a 2D titania overlayer consisting of a single layer of TiO₄ tetrahedra resides directly on the last (SrTiO)⁴⁺ plane.²³ The tetrahedra share oxygen corners and form networks of rings of variable sizes. For

example, six- and ten-membered rings are found on the SrTiO₃(110)-(4 × 1) surface. (See Figure 1b.)²³ The six-membered ring has a diameter of 5.5 Å, providing a perfect site for accommodating single Sr adatoms.²⁶ The Sr adatoms (Figure 1a) are an integral part of the structure²⁶ because they assist in compensating the polarity inherent in the (110)

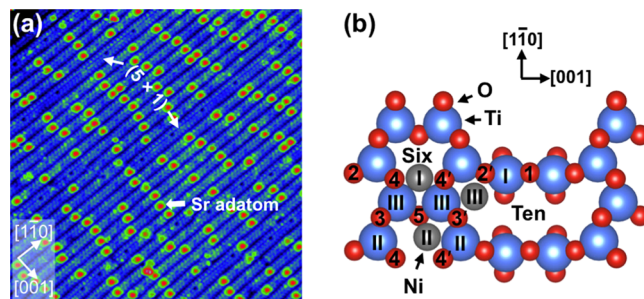


Figure 1. (a) STM image ($30 \times 30 \text{ nm}^2$, $V_{\text{sample}} = +2.0 \text{ V}$, $I_{\text{tunnel}} = 0.3 \text{ nA}$) of the SrTiO₃(110)-(4 × 1) surface. Labeled are Sr adatoms as well as a few stripes that form the (5 × 1) reconstruction.²⁶ (b) Top view of the SrTiO₃(110)-(4 × 1) surface. Ti and O atoms are shown in blue and red, respectively. Positions (I–III) for Ni adatoms (gray), attached to surface O atoms, have the most favorable adsorption energies according to DFT calculations.

Received: June 23, 2014

Revised: July 29, 2014

Published: August 2, 2014

surface. The Sr adatoms are well-dispersed and have remarkably high thermal stability. They thus could serve as nucleation centers and guide the growth of an array of noble-metal nanostructures.²⁷ We explore the formation of Ni adatoms on the 2D porous titania structure on the SrTiO_3 surface. Ni/ SrTiO_3 can be considered as a model system to investigate single-atom catalysis in, for example, water splitting.²⁸ Scanning tunneling microscopy (STM) measurements show that two types of single Ni adatoms adsorb at the six- and ten-membered rings, respectively. Photoemission spectroscopy (PES) experiments show that the Ni adatoms introduce an in-gap state and an upward band bending. Experimental and theoretical results suggest that the Ni adatoms are positively charged.

METHODS

STM experiments were performed in an UHV system with a SPECS Aarhus STM at room temperature (RT).²⁹ Synchrotron radiation PES experiments were performed at beamline I311 at the MAX IV Laboratory.³⁰ The pressure in both UHV systems was better than 1×10^{-10} mbar. Nb-doped (0.5 wt %) SrTiO_3 single crystals ($5 \text{ mm} \times 5 \text{ mm} \times 0.5 \text{ mm}$) were purchased from CrysTec, Germany. A clean surface was prepared by cycles of Ar^+ sputtering (1 keV, 5 μA , 10 min), followed by annealing in O_2 at pressures of 2×10^{-6} mbar at 1000 °C for 1 h.³¹ The samples were heated by electron bombardment (13 mA, 900 V) at the back, and the temperature was monitored with an infrared pyrometer. High-purity (99.999%) Ni metal was deposited on the surface at RT by an e-beam evaporator (Omicron EFM3). The deposition rate of 0.05 Å/min was calibrated using a quartz crystal microbalance. Spin-polarized density functional theory (DFT) calculations were carried out with the “Vienna ab initio simulation package” (VASP) code.^{32,33} We adopted the projector-augmented-wave method³⁴ and the Perdew–Burke–Ernzerhof functional³⁵ with a kinetic energy cutoff of 600 eV for plane waves. A Monkhorst–Pack k -point mesh ($2 \times 3 \times 1$) was used. The surface structure was modeled with a supercell that was symmetric along the [110] direction and consisted of a nine-layer slab separated by a vacuum layer of 12 Å. The atoms in the central three layers were fixed, and the other atoms were allowed to relax until the force on each atom was <0.02 eV/Å. Simulated STM images were generated with the Tersoff–Hamann approximation³⁶ by integrating the local density of states from the Fermi level to 1.5 eV above the conduction band edge. To take electronic correlation into account, we applied an additional on-site Coulomb repulsion term with $U_{\text{eff}} = 4.5/5.5$ eV to the Ti/Ni 3d states, respectively.

RESULTS

STM images of the $\text{SrTiO}_3(110)-(4 \times 1)$ surface exhibit quasi-1-D stripes along the [110] direction.³⁷ (See Figure 1a.) Each (4×1) stripe contains two bright rows of periodic dots, corresponding to the Ti_{II} and Ti_{III} atoms in the six-membered rings.^{26,38} (See Figure 1b.) The stripes are separated by a dark trench originating from the Ti_{I} atoms in the ten-membered rings. Single Sr adatoms with a typical apparent height of 240 pm are located in the middle of the six-membered rings, bonded to four oxygen atoms. (See Figures 1b and 2b.)²⁶

In Figure 2a, we present an empty-state STM image following deposition of 0.01 Å Ni on the $\text{SrTiO}_3(110)$ surface at RT. In addition to Sr adatoms, two types of bright protrusions are observed. Each of these protrusions has the

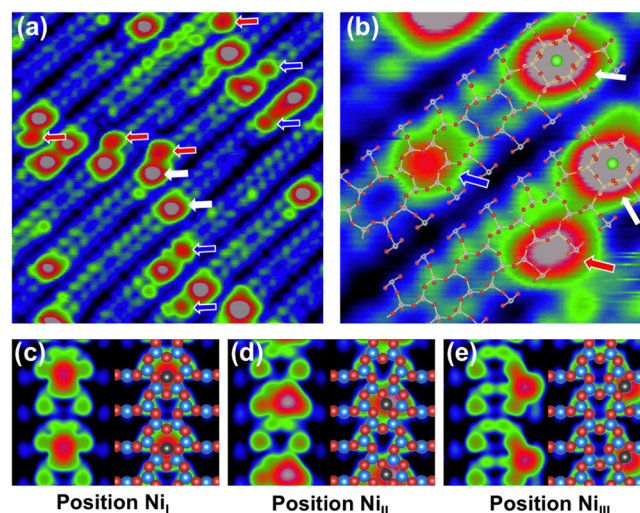


Figure 2. (a) STM image ($10 \times 10 \text{ nm}^2$, $V_{\text{sample}} = +2.0 \text{ V}$, $I_{\text{tunnel}} = 0.3 \text{ nA}$) of 0.01 Å Ni deposited on the $\text{SrTiO}_3(110)$ surface at RT. Marked with arrows are Sr atoms (white) and Ni atoms at the center (blue) and side (red) of the rows. (b) High-resolution STM image ($3.2 \times 3.2 \text{ nm}^2$, $V_{\text{sample}} = +2.0 \text{ V}$, $I_{\text{tunnel}} = 0.3 \text{ nA}$) with a structural model superimposed. (c–e) DFT-simulated STM images of single Ni adatoms adsorbed at the center (c) and off-center (d) of the rows (in a six-membered ring) and at the side (e) of the row (in a ten-membered ring).

same adsorption site and an apparent height of ~150 pm, and thus we conclude that each bright protrusion contains only one Ni atom. One type of Ni adatoms is located at the side of the (4×1) stripes (labeled with red arrows in Figure 2a); the other one appears at the center of the stripes, similar to the Sr adatoms but with smaller size (labeled with blue arrows in Figure 2a). Both types of Ni adatoms prefer to adsorb close to the intrinsic Sr adatoms. By superimposing a structural model on a high-resolution STM image, it is apparent that the center Ni adatom is located in a six-membered ring, whereas the side Ni adatom is located at the corner of a ten-membered ring. (See the red and blue arrows in Figure 2b.)

To determine the adsorption sites and energies, we have performed DFT calculations of Ni adatoms at various sites of the $\text{SrTiO}_3(110)-(4 \times 1)$ surface. (See Figure 1b.) A Ni atom (Ni_{I}) attached between O₄ and O_{4'} atoms in the six-membered ring constitutes the most favorable configuration with an adsorption energy of 1.1 (−3.4) eV with the reference to a Ni atom in the bulk fcc lattice (gas phase).³⁹ (See Figure 1b and Table 1.) The adsorption energy is ~0.3 eV less favorable when the Ni atom is placed between O_{4'} and O₅ atoms in the six-membered ring (Ni_{II}) or between O_{2'} and O_{3'} atoms in the ten-membered ring (Ni_{III}). (See Figure 1b.) All other configurations are energetically less favorable, with a more than 1 eV higher adsorption energy (not shown here). Note the clear dependence between bond length and adsorption energy; for example, the shorter the bond length, the larger the adsorption energy. In simulated STM images, the Ni adatoms are present as bright protrusions in Figure 2c–e. We conclude that the Ni_{I} and Ni_{III} adatoms observed in Figure 2b reside in center positions (in six-membered rings) and side positions (in ten-membered rings), respectively.

Figure 3a shows an STM image after deposition of 0.05 Å Ni at RT. Ni single adatoms are again present and adsorbed near the intrinsic Sr adatoms, forming well-dispersed arrays.

Table 1. Characterization of Adsorption Configurations of Ni Adatom on the $\text{SrTiO}_3(110)$ - (4×1) Surface^a

configurations	I	II	III
$E_{\text{ads}}^{\text{bulk}}$	1.11	1.49	1.38
$E_{\text{ads}}^{\text{gas}}$	-3.38	-3.0	-3.1
Ni–O bonding length	1.790, 1.790	1.828, 1.839	1.819, 1.832
bonding angle	172	162	168
height	0.801	0.468	0.596
magnetic moments (μ_B)	0.484	0.927	0.21
Bader charge	+0.30	+0.60	+0.20

^a Listed are adsorption energy E_{ads} (eV/Ni atom), referenced to bulk Ni and Ni in the gas phase, respectively,³⁹ the length of the Ni–O bond (Å), the O–Ni–O bonding angle (deg), the height of the Ni atom (Å) compared with the surface plane of the Ti_1 atom, the magnetic moment (μ_B), as well as the Bader charge analysis for Ni adatoms in the three configurations shown in Figure 1. The calculations were done within the GGA+U scheme.

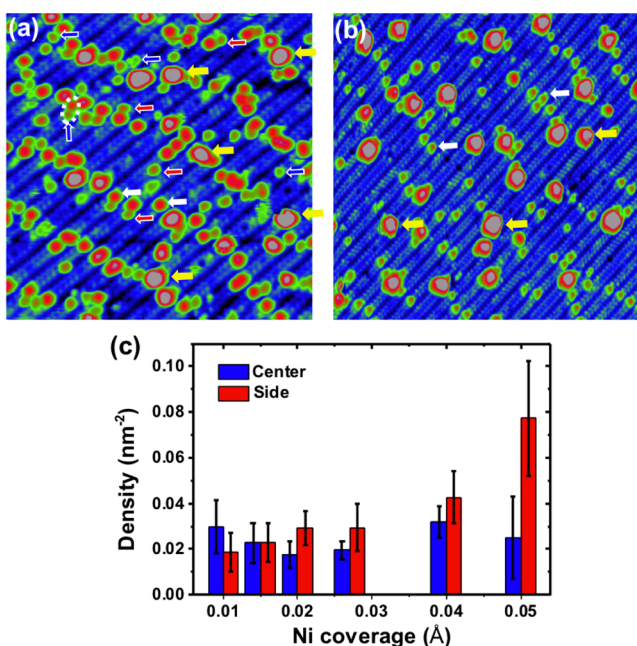


Figure 3. (a) STM image ($20 \times 20 \text{ nm}^2$, $V_{\text{sample}} = +1.6 \text{ V}$, $I_{\text{tunnel}} = 0.4 \text{ nA}$) of 0.05 \AA Ni deposited on the $\text{SrTiO}_3(110)$ surface at RT. Marked with arrows are Sr atoms (white) and Ni atoms at the center (blue) and side (red) of the rows and clusters (yellow). (b) STM image ($30 \times 30 \text{ nm}^2$, $V_{\text{sample}} = +2.0 \text{ V}$, $I_{\text{tunnel}} = 0.3 \text{ nA}$) after mild annealing 0.1 \AA Ni deposited on the surface at RT. Marked with arrows are Sr atoms (white) and Ni clusters (yellow). (c) Histogram of the density of Ni adatoms adsorbed at center and side rows of the $\text{SrTiO}_3(110)$ - (4×1) surface for various Ni coverages.

Statistics over a number of STM images (Figure 3c) show that Ni adatoms prefer the center position ($0.029 \pm 0.011 \text{ nm}^{-2}$) to the side position ($0.018 \pm 0.008 \text{ nm}^{-2}$) at low coverage. As the coverage increases, the density of the side Ni adatoms increases to $0.077 \pm 0.025 \text{ nm}^{-2}$, while the density of the center Ni adatom almost stays constant ($0.025 \pm 0.018 \text{ nm}^{-2}$). In addition, clusters with apparent heights ranging from 300 to 400 pm start to form. These clusters appear along the Sr meandering lines, attributed to Ni atoms adsorbing on the Sr adatoms (labeled with yellow arrows in Figure 3a).

Figure 4a shows the Ni 2p core-level photoemission spectra of a Ni coverage of 0.1 \AA on the $\text{SrTiO}_3(110)$ - (4×1) surface. For the surface with Ni clusters, the Ni 2p_{3/2} peak is positioned

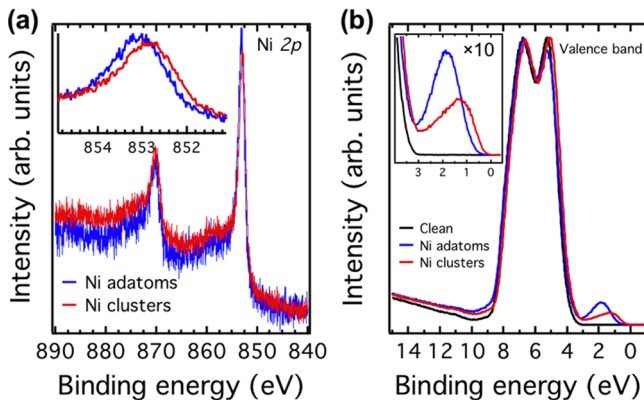


Figure 4. (a) Ni 2p core-level photoemission spectra of 0.1 \AA Ni adatoms (blue) and clusters (red) on the $\text{SrTiO}_3(110)$ - (4×1) surface. The inset shows a shift of the spectra by 0.2 eV . (b) Valence-band photoemission spectra of the clean surface (black) and surface with 0.1 \AA Ni adatoms (blue) and Ni clusters (red). The inset shows the surface states located at 1.9 and 1.3 eV below E_F in the gap region for adatoms and clusters, respectively. The core-level and valence-band spectra were measured with photon energies of 1000 and 65 eV , respectively. All spectra were taken at RT.

at 852.8 eV ; for the adatoms it is shifted by 0.2 eV to a higher binding energy of 853.0 eV . (See the inset of Figure 4a.)

To further characterize the electronic structure, we performed valence-band PES measurements. (See Figure 4b.) The valence band of the clean surface shows mainly O 2p-derived features. The valence band maximum is located at 3.2 eV below the Fermi level, and no surface states are observed in the band-gap region. (See the inset in Figure 4b.)^{21,29} After depositing Ni adatoms, the whole spectrum shifts slightly to lower binding energy, and an in-gap state with a binding energy of 1.9 eV is observed. (See the blue curve in the inset of Figure 4b.) On the surface with Ni clusters, an in-gap state appears at a binding energy of 1.3 eV .

DISCUSSION

The DFT results in Table 1 predict that the center Ni adatom is more favorable than the side configuration, which is in accord with the STM results for Ni low coverages. Two side positions can be occupied in a (4×1) unit cell, while just one position is available for the center Ni_1 adatom. (See the structural model in Figure 1b.) This two-fold side adsorption position can simply explain the experimental observation of the higher density of side Ni adatom when increasing the Ni coverage. (See Figure 3c.)

Note that the adsorption energy for all adatom configurations is positive with respect to a Ni atom in bulk fcc lattice. (See Table 1.) This implies that it is thermodynamically more favorable for Ni to form clusters on the $\text{SrTiO}_3(110)$ surface. This is consistent with the experimental results that Ni adatoms can change into clusters (with apparent heights of $\sim 600 \text{ pm}$) upon mild annealing ($< 300 \text{ }^\circ\text{C}$) in UHV. (See Figure 3b.) However, single Ni adatoms are preferred to form on the surface, even at RT. On the one hand, Ni vapor will adsorb on the surface as single adatoms first. On the other hand, sintering of Ni adatoms is kinetically hindered on the surface. This indicates that the nanopores on the SrTiO_3 - (4×1) surface play an important role for anchoring and stabilizing single adatoms.

Although the origin of in-gap states on SrTiO_3 is still under debate,^{40,71} these states typically appear at a binding energy of

1.3 eV, for example, through electron doping with atomic hydrogen or oxygen vacancies.^{29,42} Note that in these cases the formation of in-gap states is accompanied by a downward surface band bending due to electrons confined in the near-surface region.²¹ However, the in-gap state observed here, especially induced by Ni adatoms, is different from previous ones. On the Ni adatom surface, the in-gap state locates at 1.9 eV instead of 1.3 eV below E_F . In addition, the band bends upward (see Figure 6), which is opposite to the downward band bending observed in refs 21 and 29. Furthermore, a clear size dependence for the in-gap states is observed (see Figure 4b), suggesting that the in-gap states are originated from the deposited Ni on the surface.

To complement the photoemission spectra and obtain an understanding of the electronic properties of the Ni adatoms on the $\text{SrTiO}_3(110)-(4 \times 1)$ surface, we have calculated the density of states for the most stable configuration of the Ni_I adatom. (See Figure 5.) The most relevant feature is the

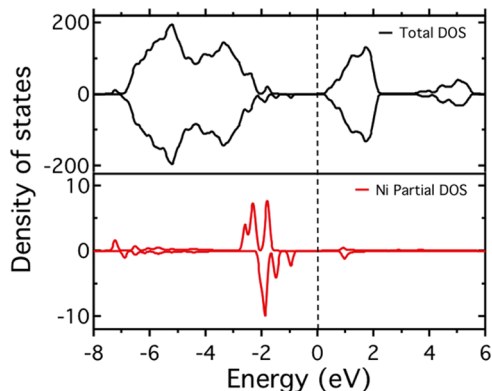


Figure 5. PBE+U valence and conduction band density of states of the Ni_I adatom on the $\text{SrTiO}_3(110)-(4 \times 1)$ surface. The upper and lower panels show the total and Ni partial density of states, respectively.

appearance of in-gap states right above the valence-band maximum, in line with the photoemission data. These states mainly originate from the Ni 3d orbitals and locate on the surface. Because they are below the Fermi level (see the lower panel of Figure 5), electrons from Nb dopant atoms in the SrTiO_3 layers can transfer into the surface states, and an upward band bending occurs. This is consistent with the experimental results that valence-band and O 1s core-level spectra shift to lower binding energies after depositing Ni adatoms. (See Figures 4a and 6a.)

The charge state of single adatoms on oxide supports is important for their reactivity;⁴ for example, both experimental and theoretical results have suggested that charged Au metal adatoms reduce the adsorption energy of small molecules as well as activation barriers for selected reactions.⁴³ The charge state of the Ni adatom is tentatively assigned to positive as the Ni 2p core-level spectrum shifts to higher binding energy in Figure 4a; however, caution is required due to final state effects in core-level PES.⁴⁴ Further insight into the Ni charge state can be obtained from the Bader charge analysis on the basis of the DFT calculations. Table 1 lists the Bader charges for the Ni atom for the preferred configurations and the corresponding magnetic moment within GGA+U scheme. It reveals that positively charged Ni adatoms are formed with Bader charges of +0.3 and +0.2 for the Ni_I and Ni_{III} adatom, respectively. Note that in DFT calculations we do not consider *n*-type doped

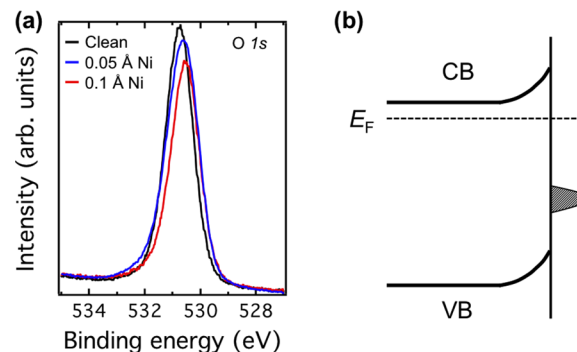


Figure 6. (a) Comparison of O 1s core-level photoemission spectra of clean surface (black) and surfaces with 0.05 Å (blue) and 0.1 Å (red) Ni adatoms. The spectra are shifted 0.2 eV to lower binding energy after depositing Ni. All spectra were taken with the photon energy of 605 eV at RT. (b) Schematic diagram of the upward surface band bending induced by Ni adatom on the $\text{SrTiO}_3(110)-(4 \times 1)$ surface.

SrTiO_3 samples were used in our experiments. Correspondingly, the magnetic moment of 0.5 and 0.2 μ_B is found for the Ni_I and Ni_{III} adatom, respectively. Apparently, the magnetic moment of the Ni atom is reduced but not completely quenched compared with the magnetic moment of 0.6 μ_B of bulk fcc Ni.

CONCLUSIONS

In summary, we demonstrate that single Ni adatoms can be stabilized at the 2D porous titania on the $\text{SrTiO}_3(110)$ surface at RT. Two types of Ni adatoms are formed by anchoring into the six- and ten-member nanopores, respectively. The Ni adatoms induce surface states at a binding energy of 1.9 eV and result in an upward band bending. Experimental and theoretical results suggest that Ni adatoms could be positively charged. Our study creates well-dispersed single-adatom arrays on a well-characterized oxide support, providing a model system to investigate single adatom catalytic and magnetic properties.

AUTHOR INFORMATION

Corresponding Authors

*Z.W.: E-mail: zwang@iap.tuwien.ac.at

*U.D.: E-mail: diebold@iap.tuwien.ac.at

Notes

The authors declare no competing financial interest.

ACKNOWLEDGMENTS

This work was supported by the Austrian Science Fund (FWF) under Project No. F45 and the ERC Advanced Research Grant “OxideSurfaces”. R.B. acknowledges support from the Doctoral College “Solids for Function”. The computational results presented have been achieved using the Vienna Scientific Cluster (VSC).

REFERENCES

- (1) Ternes, M.; Heinrich, A. J.; Schneider, W.-D. Spectroscopic Manifestations of the Kondo Effect on Single Adatoms. *J. Phys.: Condens. Matter.* **2009**, *21*, 053001.
- (2) Wiesendanger, R. Single-atom Magnetometry. *Curr. Opin. Solid State Mater. Sci.* **2011**, *15*, 1–7.
- (3) Yang, X.-F.; Wang, A.; Qiao, B.; Li, J.; Liu, J.; Zhang, T. Single-Atom Catalysts: A New Frontier in Heterogeneous Catalysis. *Acc. Chem. Res.* **2013**, *46*, 1740–1748.

- (4) Qiao, B.; Wang, A.; Yang, X.; Allard, L. F.; Jiang, Z.; Cui, Y.; Liu, J.; Li, J.; Zhang, T. Single-atom Catalysis of CO Oxidation Using Pt₁/FeOx. *Nat. Chem.* **2011**, *3*, 634–641.
- (5) Lin, J.; Wang, A.; Qiao, B.; Liu, X.; Yang, X.; Wang, X.; Liang, J.; Li, J.; Liu, J.; Zhang, T. Remarkable Performance of Ir₁/FeO_x Single-Atom Catalyst in Water Gas Shift Reaction. *J. Am. Chem. Soc.* **2013**, *135*, 15314–15317.
- (6) Moses-DeBusk, M.; Yoon, M.; Allard, L. F.; Mullins, D. R.; Wu, Z.; Yang, X.; Veith, G.; Stocks, G. M.; Narula, C. K. CO Oxidation on Supported Single Pt Atoms: Experimental and ab Initio Density Functional Studies of CO Interaction with Pt Atom on θ -Al₂O₃(010) Surface. *J. Am. Chem. Soc.* **2013**, *135*, 12634–12645.
- (7) Kaden, W. E.; Wu, T.; Kunkel, W. A.; Anderson, S. L. Electronic Structure Controls Reactivity of Size-Selected Pd Clusters Adsorbed on TiO₂ Surfaces. *Science* **2009**, *326*, 826–829.
- (8) Novotny, Z.; Argentero, G.; Wang, Z.; Schmid, M.; Diebold, U.; Parkinson, G. S. Ordered Array of Single Adatoms with Remarkable Thermal Stability: Au/Fe₃O₄(001). *Phys. Rev. Lett.* **2012**, *108*, 216103.
- (9) Giordano, L.; Pacchioni, G.; Gonikowski, J.; Nilius, N.; Rienks, E. D. L.; Freund, H.-J. Charging of Metal Adatoms on Ultrathin Oxide Films: Au and Pd on FeO/Pt(111). *Phys. Rev. Lett.* **2008**, *101*, 026102.
- (10) Nilius, N. Properties of Oxide Thin Films and Their Adsorption Behavior Studied by Scanning Tunneling Microscopy and Conductance Spectroscopy. *Surf. Sci. Rep.* **2009**, *64*, 595–659.
- (11) Parkinson, G. S.; Novotny, Z.; Argentero, G.; Schmid, M.; Pavleček, J.; Kosak, R.; Blaha, P.; Diebold, U. Carbon Monoxide-induced Adatom Sintering in a Pd-Fe₃O₄ Model Catalyst. *Nat. Mater.* **2013**, *12*, 724–728.
- (12) Martinez, U.; Jerratsch, J.-F.; Nilius, N.; Giordano, L.; Pacchioni, G.; Freund, H.-J. Tailoring the Interaction Strength Between Gold Particles and Silica Thin Films via Work Function Control. *Phys. Rev. Lett.* **2009**, *103*, 056801.
- (13) Jerratsch, J.-F.; Nilius, N.; Topwal, D.; Martinez, U.; Giordano, L.; Pacchioni, G.; Freund, H.-J. Stabilizing Monomeric Iron Species in a Porous Silica/Mo(112) Film. *ACS Nano* **2010**, *4*, 863–868.
- (14) Ulrich, S.; Nilius, N.; Freund, H.-J.; Martinez, U.; Giordano, L.; Pacchioni, G. Realization of an Atomic Sieve: Silica on Mo(112). *Surf. Sci.* **2009**, *603*, 1145–1149.
- (15) Weissenrieder, J.; Kaya, S.; Lu, J.-L.; Gao, H.-J.; Shaikhutdinov, S.; Freund, H.-J.; Sierka, M.; Todorova, T. K.; Sauer, J. Atomic Structure of a Thin Silica Film on a Mo(112) Substrate: A Two-Dimensional Network of SiO₄ Tetrahedra. *Phys. Rev. Lett.* **2005**, *95*, 076103.
- (16) Ohtomo, A.; Hwang, H. Y. A High-mobility Electron Gas at the LaAlO₃/SrTiO₃ Heterointerface. *Nature* **2004**, *427*, 423–426.
- (17) Kan, D.; Terashima, T.; Kanda, R.; Masuno, A.; Tanaka, K.; Chu, S.; Kan, H.; Ishizumi, A.; Kanemitsu, Y.; Shimakawa, Y.; et al. Blue-light Emission at Room Temperature from Ar⁺-irradiated SrTiO₃. *Nat. Mater.* **2005**, *4*, 816–819.
- (18) Ohta, H.; Kim, S.; Mune, Y.; Mizoguchi, T.; Nomura, K.; Ohta, S.; Nomura, T.; Nakanishi, Y.; Ikuhara, Y.; Hirano, M.; et al. Giant Thermoelectric Seebeck Coefficient of a Two-dimensional Electron Gas in SrTiO₃. *Nat. Mater.* **2007**, *6*, 129–134.
- (19) Kudo, A.; Miseki, Y. Heterogeneous Photocatalyst Materials for Water Splitting. *Chem. Soc. Rev.* **2009**, *38*, 253–278.
- (20) Santander-Syro, A. F.; Copie, O.; Kondo, T.; Fortuna, F.; Pailhs, S.; Weht, R.; Qiu, X. G.; Bertran, F.; Nicolaou, A.; Taleb-Ibrahimi, A.; et al. Two-dimensional Electron Gas with Universal Subbands at the Surface of SrTiO₃. *Nature* **2011**, *469*, 189–193.
- (21) Wang, Z.; Zhong, Z.; Hao, X.; Gerhold, S.; Stöger, B.; Schmid, M.; Sánchez-Barriga, J.; Varykhlov, A.; Franchini, C.; Held, K.; et al. Anisotropic Two-dimensional Electron Gas at SrTiO₃(110). *Proc. Natl. Acad. Sci. U.S.A.* **2014**, *111*, 3933–3937.
- (22) Kienzle, D. M.; Becerra-Toledo, A. E.; Marks, L. D. Vacant-Site Octahedral Tilings on SrTiO₃(001), the $(\sqrt{13} \times \sqrt{13})R33.7^\circ$ Surface, and Related Structures. *Phys. Rev. Lett.* **2011**, *106*, 176102.
- (23) Enterkin, J. A.; Subramanian, A. K.; Russell, B. C.; Castell, M. R.; Poepelmeier, K. R.; Marks, L. D. A Homologous Series of Structures on the Surface of SrTiO₃(110). *Nat. Mater.* **2010**, *9*, 245–248.
- (24) Marks, L. D.; Chiaramonti, A. N.; Tran, F.; Blaha, P. The Small Unit Cell Reconstructions of SrTiO₃(111). *Surf. Sci.* **2009**, *603*, 2179–2187.
- (25) Biswas, A.; Rossen, P. B.; Yang, C.-H.; Siemons, W.; Jung, M.-H.; Yang, I. K.; Ramesh, R.; Jeong, Y. H. Universal Ti-rich Termination of Atomically Flat SrTiO₃(001), (110), and (111) Surfaces. *Appl. Phys. Lett.* **2011**, *98*, 051904.
- (26) Wang, Z.; Li, F.; Meng, S.; Zhang, J.; Plummer, E. W.; Diebold, U.; Guo, J. Strain-Induced Defect Superstructure on the SrTiO₃(110) Surface. *Phys. Rev. Lett.* **2013**, *111*, 056101.
- (27) Zhang, Z.; Feng, J.; Wang, Z.; Yang, F.; Guo, Q.; Guo, J. Guided Growth of Ag Nanoparticles on SrTiO₃(110) Surface. *J. Chem. Phys.* **2011**, *135*, 144702.
- (28) Townsend, T. K.; Browning, N. D.; Osterloh, F. E. Overall Photocatalytic Water Splitting with NiO_x-SrTiO₃ - A Revised Mechanism. *Energy Environ. Sci.* **2012**, *5*, 9543–9550.
- (29) Wang, Z.; Hao, X.; Gerhold, S.; Novotny, Z.; Franchini, C.; McDermott, E.; Schulte, K.; Schmid, M.; Diebold, U. Water Adsorption at the Tetrahedra Titania Surface Layer of SrTiO₃(110)-(4 \times 1). *J. Phys. Chem. C* **2013**, *117*, 26060–26069.
- (30) Nyholm, R.; Andersen, J.; Johansson, U.; Jensen, B.; Lindau, I. Beamline I311 at MAX-LAB: a VUV/Soft X-ray Undulator Beamline for High Resolution Electron Spectroscopy. *Nucl. Instrum. Methods Phys. Res., Sect. A* **2001**, *467*, 520–524.
- (31) Wang, Z.; Wu, K.; Guo, Q.; Guo, J. Tuning the Termination of the SrTiO₃(110) Surface by Ar⁺ Sputtering. *Appl. Phys. Lett.* **2009**, *95*, 021912.
- (32) Kresse, G.; Hafner, J. *Ab initio* Molecular Dynamics for Open-Shell Transition Metals. *Phys. Rev. B* **1993**, *48*, 13115–13118.
- (33) Kresse, G.; Furthmüller, J. Efficiency of *ab-initio* Total Energy Calculations for Metals and Semiconductors Using a Plane-Wave Basis Set. *Comput. Mater. Sci.* **1996**, *6*, 15–50.
- (34) Blöchl, P. E. Projector augmented-wave method. *Phys. Rev. B* **1994**, *50*, 17953–17979.
- (35) Perdew, J. P.; Burke, K.; Ernzerhof, M. Generalized Gradient Approximation Made Simple. *Phys. Rev. Lett.* **1996**, *77*, 3865–3868.
- (36) Tersoff, J.; Hamann, D. R. Theory and Application for the Scanning Tunneling Microscope. *Phys. Rev. Lett.* **1983**, *50*, 1998–2001.
- (37) Wang, Z.; Yang, F.; Zhang, Z.; Tang, Y.; Feng, J.; Wu, K.; Guo, Q.; Guo, J. Evolution of the Surface Structures on SrTiO₃(110) Tuned by Ti or Sr Concentration. *Phys. Rev. B* **2011**, *83*, 155453.
- (38) Li, F.; Wang, Z.; Meng, S.; Sun, Y.; Yang, J.; Guo, Q.; Guo, J. Reversible Transition Between Thermodynamically Stable Phases with Low Density of Oxygen Vacancies on the SrTiO₃(110) Surface. *Phys. Rev. Lett.* **2011**, *107*, 036103.
- (39) The adsorption energy has been evaluated with respect to the nickel metal in fcc lattice/gas phase and is defined as $E_{\text{ads}}(\text{Ni}) = 1/2[E_{\text{tot}}(\text{Ni}/\text{slab}) - 2E_{\text{Ni}} - E_{\text{tot}}(\text{slab})]$. Here $E_{\text{tot}}(\text{Ni}/\text{slab})$ is the total energy of Ni-slab system in the equilibrium state, $E_{\text{tot}}(\text{slab})$ is the total energy of clean slab system, and E_{Ni} is the energy of Ni in fcc lattice/gas phase. With this definition, more negative values reflect a stronger interaction of the Ni atom with the SrTiO₃ surface.
- (40) Fujimori, A.; Bocquet, A.; Morikawa, K.; Kobayashi, K.; Saitoh, T.; Tokura, Y.; Hase, I.; Onoda, M. Electronic Structure and Electron-phonon Interaction in Transition Metal Oxides with d⁰ Configuration and Lightly Doped Compounds. *J. Phys. Chem. Solids* **1996**, *57*, 1379–1384.
- (41) Ishida, Y.; Eguchi, R.; Matsunami, M.; Horiba, K.; Taguchi, M.; Chainani, A.; Senba, Y.; Ohashi, H.; Ohta, H.; Shin, S. Coherent and Incoherent Excitations of Electron-Doped SrTiO₃. *Phys. Rev. Lett.* **2008**, *100*, 056401.
- (42) D'Angelo, M.; Yukawa, R.; Ozawa, K.; Yamamoto, S.; Hirahara, T.; Hasegawa, S.; Silly, M. G.; Sirotti, F.; Matsuda, I. Hydrogen-Induced Surface Metallization of SrTiO₃. *Phys. Rev. Lett.* **2012**, *108*, 116802.
- (43) Fang, H.-C.; Li, Z. H.; Fan, K.-N. CO Oxidation Catalyzed by a Single Gold Atom: Benchmark Calculations and the Performance of DFT Methods. *Phys. Chem. Chem. Phys.* **2011**, *13*, 13358–13369.

(44) Tao, J.; Pan, J.; Huan, C.; Zhang, Z.; Chai, J.; Wang, S. Origin of XPS Binding Energy Shifts in Ni Clusters and Atoms on Rutile TiO₂ Surfaces. *Surf. Sci.* **2008**, *602*, 2769–2773.